(Received 25 September 2023, Accepted 26 February 2024, Scheduled 9 March 2024)

Innovative Methodology to Improve Flexible Antenna Percentage V-Folding Performance

Ayyala K. A. Kumar[1,*], Atul Thakur[1], Shabi Baccar[2], Hugerles S. Silva[3], Preeti Thakur[1], Glauco Fontgalland[4], Yong Zhou[5], and Blaise Ravelo[5]

[1] *Centre for Nanotechnology, Amity University, Haryana Gurgaon, India*
[2] *Electronics and Systems Department, Normandie University UNIROUEN, ESIGELEC, IRSEEM Saint-Etienne-du-Rouvray, France*
[3] *Departamento de Eletrónica, Telecomunicações e Informática Instituto de Telecomunicações, Universidade de Aveiro, Campus Universitário de Santiago, 3810-193 Aveiro, Portugal*
[4] *Applied Electromagnetic and Microwave Lab., Federal University of Campina Grande Campina Grande/PB 58429, Brazil*
[5] *School of Electronic and Information Engineering, NUIST, Nanjing, Jiangsu, China*

ABSTRACT: The folding antennas are anticipated to become mandatory because of integration necessity according to communication object shapes. The effect of folded antennas on electromagnetic (EM) radiation is an open question for RF and microwave wireless engineers. An innovative approach to explore the flexible patch antenna (FPA) parameters through V-folding analysis is addressed for this problem. This paper is focused on the methodological approach of the FPA study by considering an innovative V-folding behavior compared to the classical flat condition. As a proof-of-concept, FPA prototypes are designed on a Kapton substrate, simulated, fabricated, and tested. A non-shifting operating frequency is achieved at 3.4 GHz for all percentage-wise folding with a flat (unfold) bandwidth about 360.8 MHz with good acceptable performance. The FPA performance prediction as reflection coefficient, efficiency, gain, and directivity versus forward and back V-folding percentage and angle are examined. The obtained result can be exploited to predict the V-folding effect on the communication performances of transceiver systems like radar, satellite, and multimedia applications.

1. INTRODUCTION

Behind the modern communication engineering progress, the investigation method of wireless technology plays a major role. Today, the industrial challenge in electronics and communication engineering exhibits in the fields with the deployment of smart wireless technologies [1–4]. Different varieties of smart devices were developed for health care, smart cities, smart homes, and smart cars [1–4]. In all aspects of this technological race, wireless communications with different conformal and performing structures are needed [5]. Relevant antenna design must be developed for different types of mobile terminals as wearable communication devices [6–11]. Technological solutions presenting technical, commercial, and socio-economic benefits are expected to follow the wireless technology progress roadmap of today's research and engineering.

Innovative design concerning the antenna topologies is needed to achieve high-performance communication. Concerning the nontrivial geometrical shape of wearable devices, a relevant design method of flexible patch antennas (FPAs) is expected. Because of design simplicity and frequency bands flexibility, simple topologies as patch antennas (PAs) [12–20] constitute solutions for wide range of wireless application as wearable devices, WiMAX base station, and even satellite payloads. One of the roadblocks for antenna design engineers is to find reliable solutions integrable into future electronic and communication devices. In this optics, research works are currently going on to identify the highest performance integrable antenna by considering uncommon geometrical shapes, which leads to the development of flexible antennas [21–32]. Innovative flexible and robust antenna designs have been developed for different applications [26, 27]. The study of innovative antenna design on flexible substrates, such as PET (Polyethylene terephthalate) and Kapton [21, 23–25, 30, 31] is gaining attention. According to the targeted applications, geometrically flexible antenna design adapted to wearable-device shapes must be developed [6–8, 10, 11]. It can be noticed that solutions involving FPAs [24, 25, 30–33] using different substrates have become a trend.

Nevertheless, we still need to find a relevant engineering methodology to design a flexible antenna with the best communication performance [34] by considering nontrivial geometries of bending and folding [35–38]. Most bent antennas were designed on textile substrates [11, 33, 34, 38], Kapton [21, 23–25, 30, 31], and other flexible materials [26–28]. However, Kapton is one of the best low-cost polyimide film substrates for manufacturing in aircraft, spacecraft, X-rays, 3-D printing, flexible printed circuit boards (PCBs), and antennas. Moreover, Kapton has good insulation properties with extraordinary temperature stability. Kapton substrate is compact, light, and

* Corresponding author: Ayyala Kishore Ajay Kumar (kishoreajay@gmail.com).

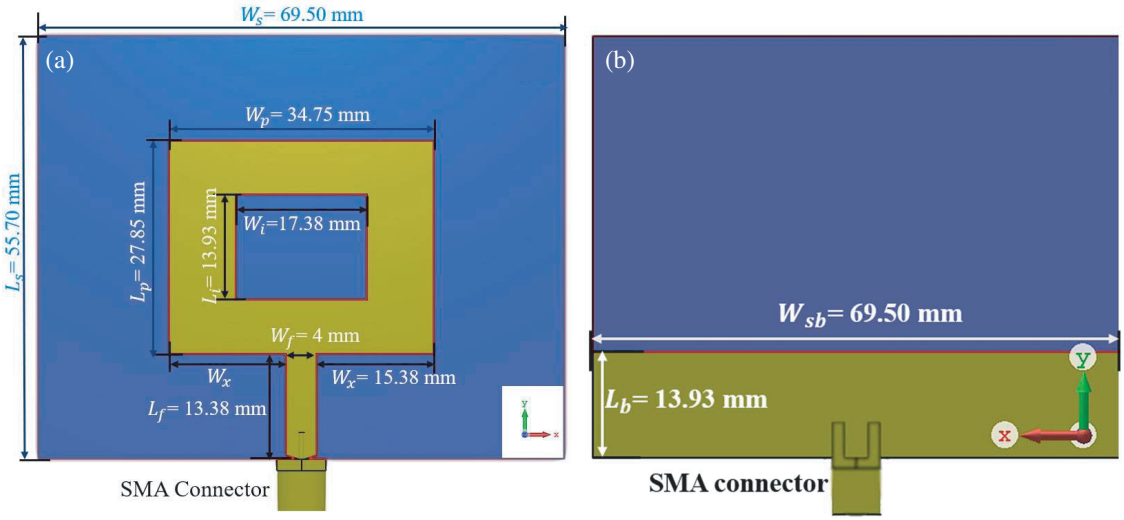

FIGURE 1. FPA design: (a) top and (b) bottom 2-D views.

has conformal design capability, including multiband and wideband performance in bent configurations.

Despite the progressive research work on flexible antenna design [21–37], further academic research is necessary to develop relevant methodology enabling radiation performances. In the present study, an innovative FPA design methodology is introduced through a wise conceptualization of folding percentage (FP) in two ways. The first one is toward the front portion (radiating patch) called front folding percentage (FFP). The other one is towards the back portion (ground plan) called back folding percentage (BFP), so we can understand the behavior of FPA folded on both sides. Investigation from 3-D electromagnetic (EM) simulations and experimental measurements of complex V-folded prototypes with fixed folded angle at 10° and monitoring the effect of entire PA called percentage wise folding (PF) different angles varied from 10% to 100% are considered in the frequency band 0.1 GHz–5 GHz. Holding the resonance frequency shift and improving the performance of parameters are challenging for all bending or folding types of PAs [34–36]. The main novelty of this research work is the development of the methodological and experimental analysis of V-folding flexible PAs. This novel approach showing the entire structure percentage-wise in FFP and BFP is explored for the first time according to the best knowledge of the authors. The PA can be used in either FFP or BFP, so the antenna attains good performance with stability. The unexpected effect of V-folding is investigated from the 3-D EM simulation process. The developed study of the FPA V-folding effect is particularly useful for different applications such as 5G and 6G RF/microwave transceivers implemented on complex geometrical shape devices. The FPA geometric deformation that leads to the desired EM effect of FFP, and BFP is developed and explained.

This paper is organized as follows:

- In Section 2, the description and methodology of V-folded FPA design engineering are investigated. The proof of concept (POC) of V-folded FPA explored in this study is designed based on a microstrip patch antenna (MPA) as a classical flat circuit. The FP concept concerning the V-folded FPA geometrical parameters is also defined.
- Section 3 focuses on the analyses of the reflection coefficient (S_{11}) and radiation simulation results from the V-folded FPA POC. The main influence of the V-folded angle and FP on the performances concerning the FFP and BFP are discussed.
- In Section 4, the improvement of V-folded FPA performance is evaluated by means of the gain (G), directivity (D), total efficiency, resonance frequency (F_r), bandwidth (BW), and S_{11}. The proposed analysis is elaborated by theoretical considerations reported previously [30, 31].
- The prototypes and challenging test setups concerning the FP are revealed in Section 5. The experimental validity is studied through a comparison of 3-D simulation and measured results.
- Section 6 presents the conclusion of this work.

2. V-FOLDED FPA DESIGN DESCRIPTION AND METHODOLOGY

The present section reveals the description and methodological investigation of the V-folded FPA design. The considered POC is designed by using the CST MWS 2018 commercial tool.

2.1. FPA Design Description

First and foremost, the FPA under study is designed with microstrip technology. The FPA POC is designed on a flexible Kapton substrate specified by the dielectric constant ε_r, loss tangent $\tan(\delta)$, and thickness h. The copper (Cu) metallization presents the thickness t and conductivity σ. The FPA constituting material physical parameters are indicated by Table 1. Fig. 1(a) and Fig. 1(b) represent the top and bottom 2-D views of FPA POCs, respectively. During the simulation and test, the proposed FPA POC is expected to operate with $R_0 = 50\,\Omega$

TABLE 1. Physical specifications of POC FPA constituting material.

Material	Designation	Parameter	Value
Kapton substrate	Dielectric constant	ε_r	3.4
	Loss tangent	$\tan(\delta)$	0.02 dB/in
	Thickness	h	0.52 mm
Copper metallization	Conductivity	σ	58 MS/s
	Thickness	t	18 µm

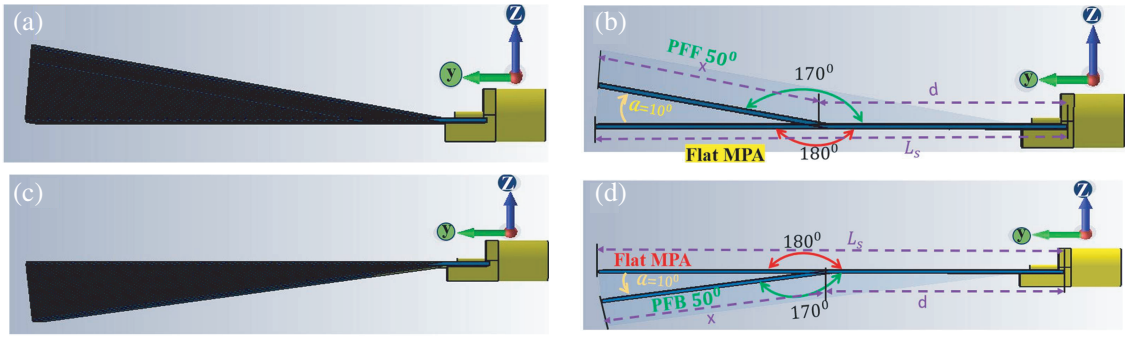

FIGURE 2. Horizontally Side views of (a) front V-folding complete samples 3D, (b) concept of front V-fold with FFP $FP = 50\%$, (c) complete samples back V-folding 3D, and (d) concept of back V-folding with BFP $FP = 50\%$.

coaxial feed via an SMA connector. The FPA geometrical shape and dimensions with length L_s and width W_s are ideally calculated from formulas available in the literature [39]. Let us denote the ratio of feed length L_f to the starting patch width W_x written as:

$$k = L_f/W_x. \tag{1}$$

By taking $c = 300,000$ km/s as the speed of light, it is worth reminding that the FPA fundamental resonance frequency is theoretically defined by [39]:

$$F_r = \frac{c}{W_p k\sqrt{2(\varepsilon_r+1)}}. \tag{2}$$

Emphatically, the FPA ideal width can be determined from resonance frequency by the relationship:

$$W_p = \frac{W_x c}{L_f F_r\sqrt{2(\varepsilon_r+1)}}. \tag{3}$$

For example, during the design phase, the targeted resonance frequency is equal to $F_r = 3.4$ GHz in a fully flat horizontal position. Therefore, one gets the FPA design geometrical parameters L_p, W_p, W_i, L_i, W_x, and L_f described by Fig. 1.

The chosen final parameters are mentioned in Table 2. The concept of FP applied to the V-folded FPA is described in the next subsection.

2.2. Conceptualization of Folding Percentage (FP)

Many research works have presented different types of bent and folded PAs for different purposes [7–29]. We can find cylindrical bent and different conformal antennas for different applications. PA bending will be required for applications like internet of things (IoT) and automobiles so that the antenna is deformed according to the shape of the device needed for communication. Deforming the MPAs into different shapes needs some deep learning through simulation tools. Deforming the antenna with a small tilt in angle will affect its performance. Folding PA changes lumped elements discussed in Section 3.2 causing changes in surface current distribution and efficiency for every PF. In the present work, a few steps are followed to implement the V-folding structure. The proposed V-FP wise concept is implemented to understand the performance of the antenna fashioned on sharp-edge devices as illustrated by Fig. 2.

Consider that the length of the antenna L_s is divided into x (after folding) and d (before folding) while the folding effect on the MPA parameters is analyzed concerning partial lengths of d and $x = L_s - d$. The expression of V-folding in percentage is a function of the ratio d knowing that $L_s = d + x$. The V-folding for the front and back control parameter as shown in Fig. 2 is defined by:

$$FP(\%) = 100\, d/L_s \tag{4}$$

The implementation of FPA as FP POC is discussed in the next subsection.

2.3. FPA POC Implementation

As a basic construction of PAs, many samples were considered during the design to achieve good performance while folding the antenna horizontally at $a = 10°$. Starting with the simple construction of a rectangular patch as shown in Fig. 1(a), it is

TABLE 2. Geometrical parameters designed FPA POC shown by Fig. 1.

Material	Designation	Parameter	Value
Substrate	Length	L_s	55.7 mm
	Width	W_s	69.5 mm
PA	Length	L_p	27.85 mm
	Width	W_p	34.75 mm
		W_x	15.38 mm
	Length	L_i	13.93 mm
	Width	W_i	17.38 mm
Feed line	Length	L_f	13.38 mm
	Width	W_f	4 mm
Ground plane metallization	Length	L_b	13.93 mm
	Width	W_{sb}	69.5 mm

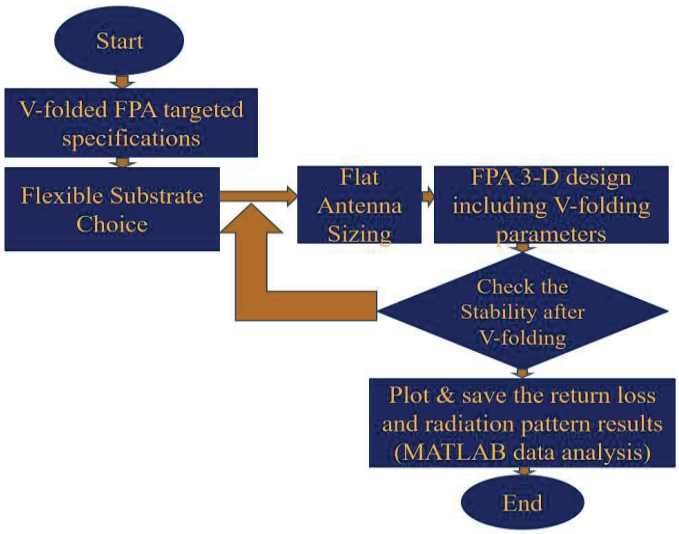

FIGURE 3. Workflow highlighting the V-folded FPA design methodology.

required that the FPA does not deteriorate its performance for every sample of FP. First, it is focused on the flat (unfold) conditions of FPA and holds good performance after folding. When the height of the substrate is increased, certain areas of radiating face iterate for the best-holding fringing effect. Finally, the reduction in the metallic surface in the ground plane is made to maintain the performance [31] and is monitored through the simulation process. It is known that small changes in FPA design will certainly change its performance. Second, focusing on the V-folded FFP and BFP samples the same steps are followed to achieve the same performance as the unfolding condition model. So, finally, the samples optimization simulation process achieves a stable (unchanged) performance, after following the methodology for all FPs. Among many factors that affect F_r like the FPA design, the substrate height, and feeding point, etc., k has strongly been considered for this simple structure. This design is restricted with a ground plane to length $L_b = 13.93$ mm and width $W_{sb} = 69.5$ mm, as shown in Fig. 1, to improve the fringing effect and increase the Kapton height four times compared to the previous structure [9, 10] to achieve stabilization in the frequency shifting while FPA is folded as shown in Fig. 1. There will be more changes in performance if the exact construction in the simulation process is neglected. The main reason to have a restricted design is to achieve flexible antenna performance with no compromise in folding during simulation.

2.4. Methodology

In this work, a qualitative antenna design method is explored without loss of accuracy. Fig. 3 summarizes the main steps of the V-folded FPA POC design. The proposed design methodology is based on the folding behavior exploration of the front and back portions of the FPA for all considered samples to achieve stability in performance. First of all, the targeted specifications and the employed flexible substrate are defined.

The ideal FPA sizing is calculated by using classical flat antenna design formulas available in the literature [39]. The 3-D design configuration of FPA structure using the simulation tool must be chosen for holding stability in the V-folded position.

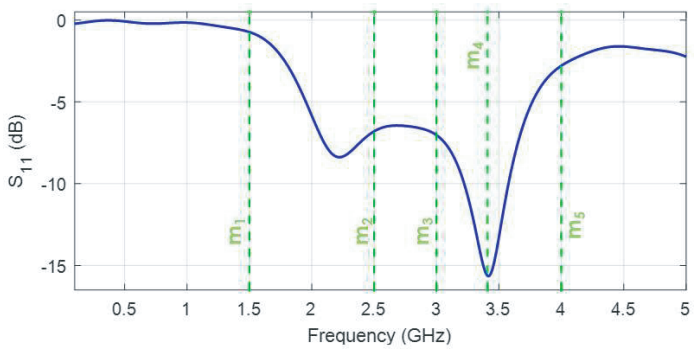

FIGURE 4. S_{11} of flat (unfold) PA shown in Fig. 2.

The challenging aspect of the V-folding study is the ability to consider every change in the ground plan dimensions (metallic bulk) and substrate height to keep the FPA best performance. To verify the design method's relevance, a study on FPA V-folding effect is elaborated in the next section.

3. EFFECT OF FPA V-FOLDING ON REFLECTION COEFFICIENT AND RADIATION PATTERN

The misunderstood effect of FPA V-folding on reflection coefficient and radiation pattern is described in the present section.

3.1. Theoretical Recall

With reference impedance $R_0 = 50\,\Omega$, based on the microstrip circuit theory, the FPA input complex impedance at operation frequency f determined from the frequency-dependent reflection coefficient S_{11} can be calculated by:

$$Z(jf) = \frac{R_0[1 + S_{11}(jf)]}{1 - S_{11}(jf)}. \tag{5}$$

Emphatically, the resistance is determined from a real part which is given by $R = \text{real}(Z)$. The inductance and capacitance calculated from extracted simulation results are the imaginary impedance, $\text{imag}(Z)$, at the specified frequency F_r in the plot by the relations:

$$L = \text{imag}(Z)/(2\pi F_r) \tag{6}$$

$$C = 1/[(2\pi F_r)^2 L]. \tag{7}$$

The radiation field is a prominent parameter for investigating the FP geometrical effect of FPA. For the analysis of the radiation result plot, the spherical coordinate system is considered for monitoring shifts in azimuthal and elevation angles, θ and φ, respectively. By denoting the radiation pattern e_{rad}, the gain and directivity are linked by the relationship [39]:

$$G(\theta, \varphi) = e_{rad} \times D(\theta, \varphi). \tag{8}$$

These expressions serve in the next subsections to the FPA effect analysis versus V-folding angle by means of reflection coefficient and radiation pattern.

3.2. Interpretation of FPA S_{11} Versus FP

Since the structure and design of the antenna are different from the original rectangular PA, the design parameters will be certainly different.

3.2.1. Analysis of Unfolded FPA S_{11}

The effect of FFP and BFP is understood through the reference S-parameters of flat (unfold) conditions as shown in Fig. 4. The analysis of unfolded PA S-parameters provides some indication points referenced by $m_{x=1,\ldots,2}$, specified from m_1 to m_5, where significant changes are observed. These points are considered and noted as the change linked to calculated lumped elements shown in Table 3. From the plot shown in Fig. 4, no resonance is observed in the frequency range of 0.1 GHz to 1.5 GHz until the m_1 point. This is mainly due to the high capacitive value. At m_2, there is a hold of resonance m_3 due to a reduction in capacitance and negligible change in inductance. There is no effect from m_2 to m_3 due to no change in inductance. Increasing the frequency, from m_3 to m_4, the resonant phenomenon is observed due to an increase in inductance. From point m_4 to m_5 we observe S_{11} plot due to an increase in inductance and a decrease in capacitance.

TABLE 3. Illustrative effect analysis through S_{11} for flat condition simulation.

m_x (S_{11})	F_r (GHz)	S_{11} (dB)	R (Ω)	L (nH)	C (pF)
m_1	1.5	-0.7	2.26	2.1	5.4
m_2	2.5	-6.69	26.76	1.9	2.1
m_3	3	-7	39.75	2.3	1.2
m_4	3.4075	-15.42	46.29	0.8	2.9
m_5	4	-2.77	31.23	4.7	0.3

It is considered that the capacitance and inductance values are complete parts of resonance occurrence with a drastic rise in resistance for all points as shown in Table 3 for all complete FFP and BFP samples. The inductance plays an important role in a sharp shoot in resonance frequency due to the dimensions of an antenna and the increase in height of a substrate. From the present discussion, two regions are considered causing res-

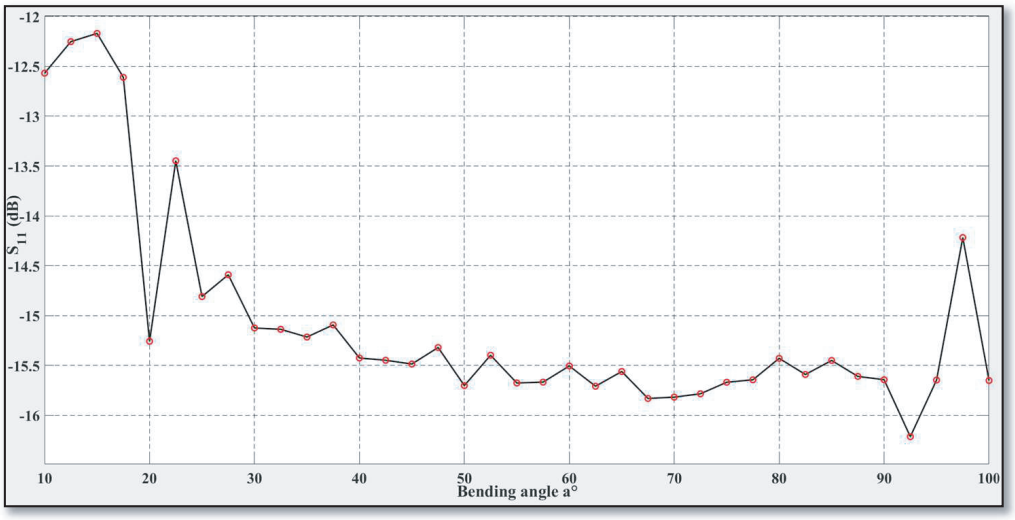

FIGURE 5. Complete S_{11} of FFP as shown in Fig. 2 for all simulated samples.

onance, the first one from m_1 to m_2 and the second one from m_3 to m_5.

3.2.2. FFP S_{11} Analysis

While folding the FPA, as shown in Fig. 3, in the front side it has no major changes with less shifting in the second region due to lumped elements, as explained above. As depicted by Fig. 5, the folding front has no impact in the first region but promises good return loss after complete folding is achieved with more than -12.5 dB. Achieving this resonance frequency with minor effect is challenging for any type of folding FPA angle a^0 by maintaining F_r within 3.4 GHz to 3.5 GHz from 10% to 100% (unfold). Here in FFP from 10% to 25% folding takes place only on feeding line L_f towards the radiating face, which has slight changes from the second region due to changes in the inductance. From 25% to 100% (unfold), there are no changes observed in S_{11} even while folding occurrence on patch radiating face stated as stabilized performance.

After completing the FFP simulation, it can be observed that $d = 15$ has a minimum of -12.1 dB at 3.48 GHz while at $d = 92.5$ it reaches a maximum of -16.22 dB at 3.41 GHz.

3.2.3. BFP S_{11} Analysis

While folding the MPA, as shown in Fig. 2(d), towards the back side, i.e., the ground plane has an effect in the first region for samples from $d = 10\%$ to 22.5% creating equal resonance at the second region. It is due to the physical folding, which is only done on feed line L_f of the radiating face, causing a decrease in capacitance. Since folding from $d = 25\%$ will be on a radiating patch, the improved inductance has a shift into a higher frequency range, as in the second region. The MPA behavior differs while folding occurs on radiating patches compared with the patch from $d = 10\%$ to 22.5%. The comparison of FFP and BFP shows a slight difference of 4% in all parameters, as shown in Fig. 6, and then is considered negligible. A slight change in L and C with folding MPA is the main reason for the minor shift. After completing the BFP simulation, it is observed that $d = 22.5\%$ has a minimum of -8.68 dB at 3.623 GHz, a multi-band behavior at 2.1 GHz, and $d = 70\%$ has a maximum of -15.77 dB at 3.41 GHz. After the S_{11} analysis, the FPA radiation pattern was also investigated as described in the following subsection.

3.3. Folding Effect on FPA Radiation

The FPA structure will radiate according to the structure folded whether it is FFP or BFP. The innovative results of the V-folding effect on the 3-D radiation pattern are analysed in the present subsection.

3.3.1. Analysis of V-Folded FPA 3-D Radiation

After CST MWS EM simulation, the 3-D plot of far-field gain radiated by the V-folded FPA is displayed in Fig. 7.

The shift is observed compared with unfold in FFP and BFP as shown in Fig. 7(a) for the flat position, and Fig. 7(b) and Fig. 7(c) for $d = 10\%$. We can see that FFP $d = 10\%$ radiates in the direction of $a = -30^\circ$ descending angle, and BFP at $d = 10\%$ radiates in the direction of $a = 30^\circ$ ascendant angle compared with unfolded FPA radiates at $a = 0^\circ$. It is observed that BFP values are slightly high for directivity and gain due to this shift in the radiating field. From the observation of the E or electric field plot of Fig. 7(d), the radiation pattern has a slight shift in azimuthal angle θ considered negligible. But the shift mostly occurred due to the polar angle φ from the above equations, and a maximum field $E_{\max} \approx 7.45$ V/m at the distance $r = 1$ m of the radiation source was obtained for the complete FPA samples observed in the simulation.

3.3.2. Discussion via Comparison between FFP and BFP Radiation

An extreme shift is observed in the FFP and BFP configurations for angle $d = 10\%$. The angular width of 3 dB in simula-

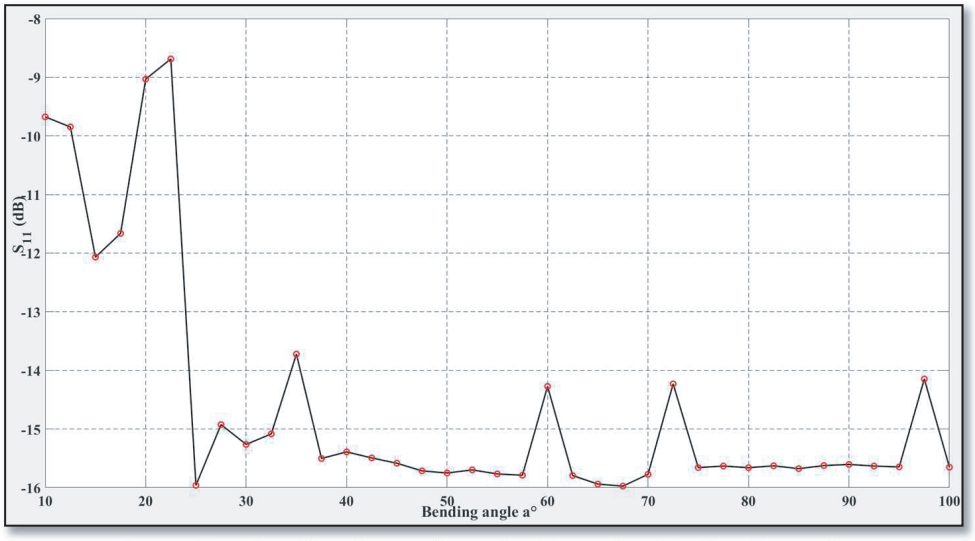

FIGURE 6. Complete S_{11} of BFP shown in Fig. 2 for simulated samples.

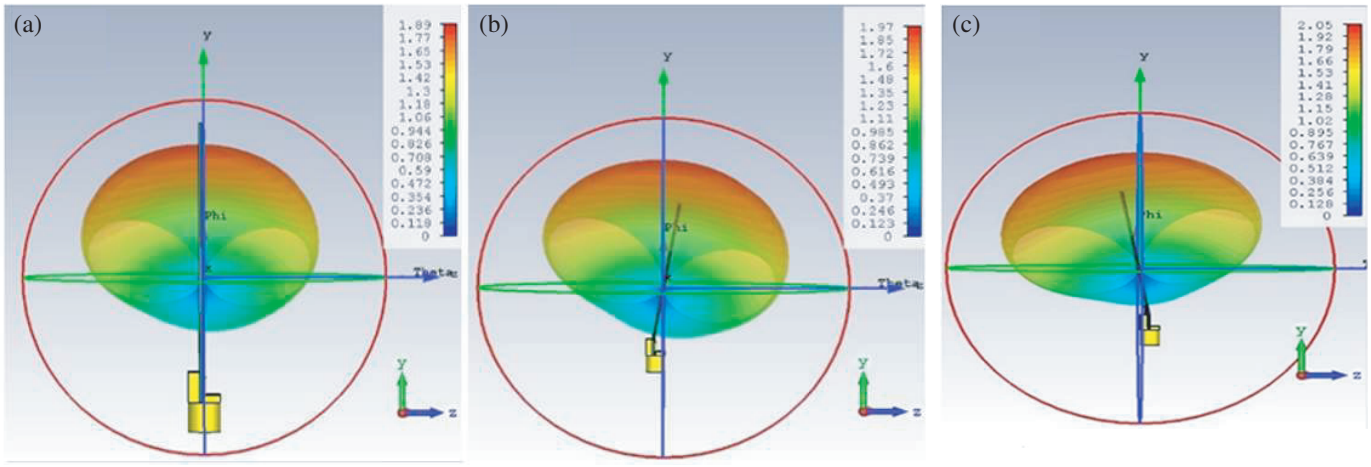

FIGURE 7. 3-D views of far-field gain (left side view), (a) flat condition, (b) $d = 10\%$ FFP front V-folding and (c) $d = 10\%$ BFP V-folding.

tion considered as half-power bandwidth (HPBW) is $a = 78.8°$ for unfolding FPA having slight changes in FFP and BFP due to change in φ. For the FFP radiation field from $-30°$ to $0°$, there is an increase of $1°$ for every sample (i.e., 2.5%) and after the FFP reaches 75%. It holds no shift in radiation due to the folding of FPA since it is done after the metallic patch surface, which is a cause of radiating. The angular width (3 dB) of all FFP samples lies between $74.5°$ and $76.5°$, which is a cause of slightly increasing gain and directivity. For the BFP radiation field from $30°$ to $0°$, there is a decrease of $1°$ for every sample (i.e., 2.5%) as illustrated by Fig. 8.

When the BFP reaches 72.5%, it holds no shift in radiation due to folding at the edge of the patch metallic surface, so radiation leak will be good. The angular width (3 dB) of all BFP samples lies between $76.5°$ and $81.5°$, which is a strong reason for a good improvement in gain and directivity. The next section is focused on the performance improvement of V-folded FPA.

4. ANALYSIS OF V-FOLDED FPA PERFORMANCE IMPROVEMENT

Based on the obtained 3-D EM simulation results, the performance improvement of the V-folded FPA under FFP and BFP configurations compared to the flat position is analyzed in the present section.

4.1. Comparison of FFP and BFP Simulated Results

The FPA previously shown by Fig. 2 was also simulated with a parametric variation of *FP*. The obtained results for assessing the antenna performance concerning the FFP and BFP positions are discussed in the present subsection. The simulation results highlight a very clear study of V-folding for every $\Delta FP = 2.5\%$ increase from $FP_{\min} = 10\%$ in the structure front and back until $FP_{\max} = 100\%$ (unfold). The accumulated results with basic characteristics are shown in Fig. 9. The initial V-folding FP is considered as 10% due to the coaxial

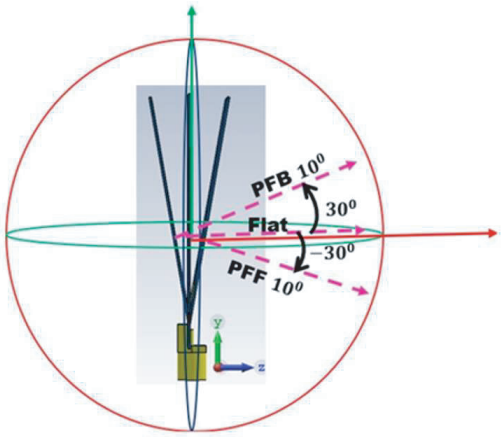

FIGURE 8. Radiation field comparison of flat FFP and BFP for $a = 10°$.

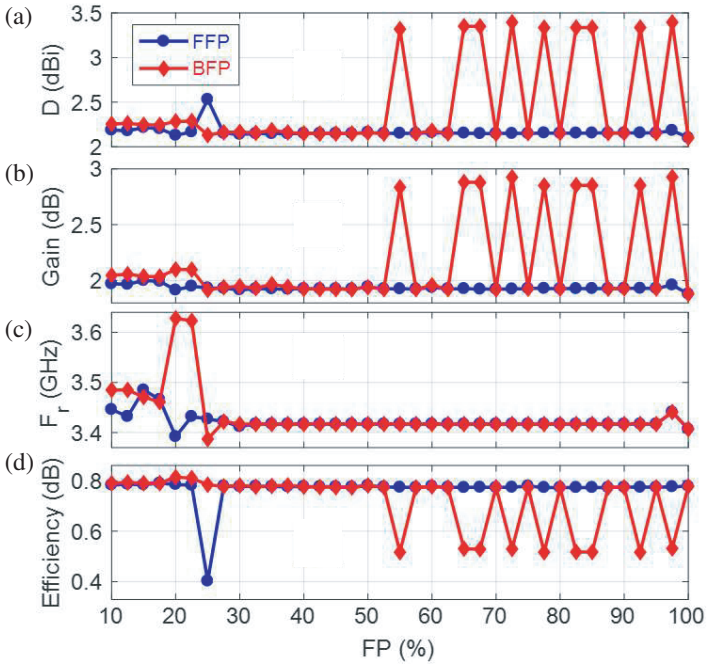

FIGURE 9. Comparison of simulated FFP and BFP (a) directivity, (b) gain, (c) resonance frequency, and (d) total efficiency. All the characteristics plotted according to simulation results are not stable from $d = 10\%$ to 25%, which is due to FP at feeding length L_f in both FFP and BFP. After feeding, once the FP is reached, stability is obtained due to proper inductance and capacitance values.

feeding interruption. A 2.5% increment for every fold allows us to follow the change. The simulation results highlight a very clear study of V-folding for every $\Delta FP = 2.5\%$ increase from $FP = 10\%$ in the structure front and back until $FP = 100\%$ (unfold) accumulated with basic characteristics shown in Fig. 9. During the computation, the FP of initial V-folding is considered as $FP = 10\%$ due to the coaxial feeding interruption. A $\Delta FP = 2.5\%$ increment for every fold allows to follow the change. Some changes are not observable compared to the previous work [31]. Important characteristics monitored by comparing FFP and BFP from the 3-D EM simulation are the directivity D, gain, resonance frequency F_r, and total efficiency as shown in Fig. 9.

All the characteristics plotted according to simulation results are not stable from $d = 10\%$ to 25%, which is due to FP at feeding length L_f in both FFP and BFP. After feeding, once the FP is reached, stability is obtained due to proper inductance and capacitance values.

4.2. Simulated Results to Improve V-Folded MPA Performance

The simulation results are required to understand the performance before measurement. The challenging improvement through FPA is simulated by the high-performance CST Studio Suite to improve performance step by step as mentioned in the methodology depicted in Fig. 1(a). Improving the performance starts from unfolding FPA expecting the performance without degradation with FFP and BFP from $PF = 10\%$ V-folding for all samples. Previous work [31] with a normal structure shows the performance and improvement in simulation af-

TABLE 4. Comparison of Flat FPA performance from my previous work.

S. No	Type of FPA	h (mm)	F_r (GHz)	S_{11} (dB)	BW (MHz)	D (dBi)	Gain (dB)
1	[31]	0.13	1.42	−22.8	31.6	5.5	−18.54
2	Trimmed ground	0.13	1.79	−1.58	-	2.14	1.72
3	Normal ground	0.26	4.26	−21.0	75.7	6.97	−7.46
4	Trimmed ground	0.26	1.84	−6.38	-	2.39	1.81
5	Normal ground	0.39	4.30	−11.4	52.8	7.03	−5.03
6	Trimmed ground	0.39	1.88	−12.7	174.7	2.16	1.93
7	Normal ground	0.52	4.36	−9.68	-	8.026	0.98
8	This paper	0.52	3.40	−15.4	360.8	2.10	1.88

ter iteration in the ground plane as shown in Table 4. In this paper, multiple simulation results for unfold antenna consider normal ground called full ground placed and trimmed ground called iterated ground up to $FP = 52.8\%$. The main intention of calculating the different heights of substrates starting from $h_{\text{min}} = 0.13\,\text{mm}$ to $h_{\text{max}} = 0.52\,\text{mm}$ is to observe the performance while simulating with the normal ground and trimmed ground. Kapton obtained in the market is 0.13 mm only, but we need to enhance the height of the substrate by about 4 times to obtain the best performance as shown in Table 4. The main reason for the observed shift and changes in performance is a fringing field effect. The 3-D EM simulation was first focused on unfolding FPA to understand and improve performance by practicing in different scenarios. As explained by Table 4, we understand that iteration of ground will hold frequency shifting for all percentage-wise folding, and an increase in height h of substrate improves the performance of parameters, especially gain. For practical validation of the obtained simulated results, an experimental investigation is discussed in the following section. Here, the thickness of the substrate is increased step by step in CST Studio for simulation results, so that with V-folding the PA can achieve stability in performance.

5. INVESTIGATION OF FPA EXPERIMENTAL RESULTS

The experimentation results in V-folded FPA highlighting the behaviors analyzed of the previous sections are discussed in the present section.

5.1. Description of FPA Prototyping

The FPA V-folding experimentation was studied by fabricating and testing prototypes presented by Fig. 10. These FPA prototypes were chosen by exhibiting good performance due to the real-time fringing field. The employed flexible substrate is Kapton polyimide readily available in different forms (adhesive, normal). The experimental tests were performed for flat FPA position (Fig. 10(a)), two cases of the FFP (Fig. 10(b) and Fig. 10(c)), and two cases of BFP (Fig. 10(b) and Fig. 10(c)) positions. For these test cases, $FP = \{10\%, 75\%\}$ was considered as indicated by Table 5. However, to increase the antenna width, glue is used for FFP and BFP (for $FP = 75\%$). For both test cases, the V-folding layer by layer since $FP = 75\%$ does not change the radiating microstrip patch. The convenience on increasing the width is that the PA will hold V-folding without any support (like a polyvinyl chloride (PVC) fixture or holder).

TABLE 5. Tested FPA prototype configurations.

Configuration	Unfolded	FFP		BFP	
Fig.	10(a)	10(b)	10(c)	10(d)	10(e)
FP	100%	10%	75%	10%	75%

5.2. Description of FPA Challenging Experimental Setup

The fabricated FPA is presented with front and side views of every FP fixed on the folding clips to hold the designed antenna for extracting the measurement results. The V-folded FPA was tested in an anechoic chamber of the EM research laboratory of the Central Research Facility IIT Delhi. During the test, the return loss was measured with an Anritsu MS2028C vector network analyzer (VNA). The FPA was also tested by using Keysight EXA signal analyzer N9010A operating from 10 Hz to 44 GHz as displayed in Fig. 11. The photographs of the experimental environment with the flat FPA prototype placed on test support are displayed in Fig. 12(a) for flat & folded FPA in Fig. 12(b). In addition, the obtained test results of V-folded FPA performance from the challenging experimentation are discussed in the following subsection.

5.3. Analyses on Simulated and Measured Performances of V-Folded FPA

Multiple simulation results for unfold antenna consider normal ground called full ground placed and trimmed ground called iterated ground up to 52.8%. The main intention of calculating the different heights of substrates starting from $h_{\text{min}} = 0.13\,\text{mm}$ to $h_{\text{max}} = 0.52\,\text{mm}$ is to observe the performance while simulating with the normal ground and trimmed ground. The Kapton provided in the market is 0.13 mm only, but we need to enhance

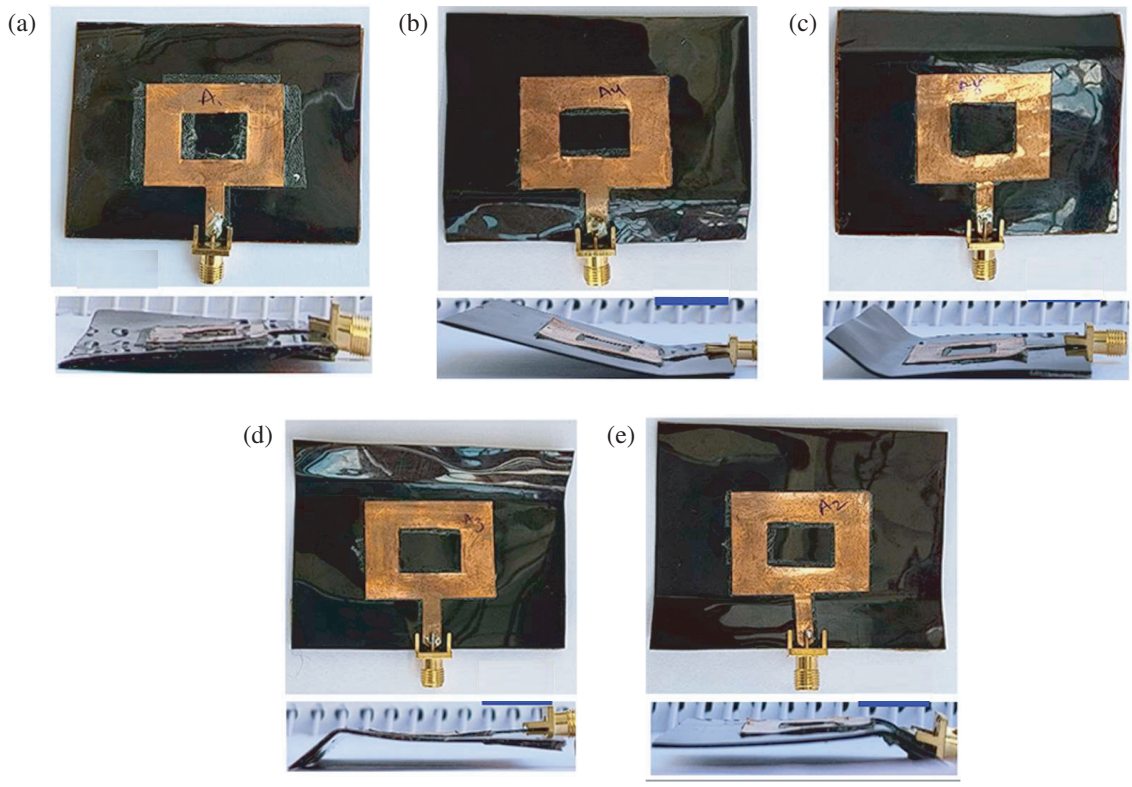

FIGURE 10. Illustration of experimented V-folded FPA positions: (a) flat (unfold), ((b) $d = 10\%$ and (c) $d = 75\%$) FFP, and ((d) $d = 10\%$ and (e) $d = 75\%$) BFP with corresponding side view.

TABLE 6. Comparison of V-folded FPA simulated and measured performances.

Approach	V-fold types	*FP* (%)	F_r (GHz)	S_{11} (dB)	*D* (dBi)	Gain (dB)
Simulation	Flat (unfold)	100	3.40	−15.65	2.10	1.88
	FFP	10	3.44	−12.56	2.18	1.97
		75	3.41	−15.66	2.15	1.92
	BFP	10	3.48	−9.67	2.25	2.04
		75	3.41	−15.65	2.15	1.92
Measurement	Flat (unfold)	100	2.74	−23.9	2.54	4.03
	FFP	10	3.34	−24.3	1.64	1.75
		75	2.08	−44.6	2.25	2.19
	BFP	10	3.40	−27.1	1.83	1.95
		75	2.23	−29.2	1.86	2.20

the height of the substrate by about 4 times to obtain the best performance as shown in Table 6.

The main reason for the shift and changes in performance observed is a fringing field effect. The 3-D EM simulation results were first focused on unfolding FPA to understand and improve performance by practicing in different scenarios. In the experimental setup, the fabricated FPA is presented with front and side views of every FP fixed on the folding clips to hold the designed antenna for extracting the measurement results. Simulation results show stabilization of F_r, gain, and D for all samples. The comparison between the simulated and measured results is addressed in Table 6. After the result analyses, a good correlation between the FPA performances such as resonance frequency, return loss, directivity, and gain concerning arbitrarily chosen $FP = \{10\%, 75\%, 100\%\}$ is found. The slight differences between the noticed parameters are mainly due to the test setup's mechanical imperfections and the substrate material discrepancies. It is noteworthy that the copper sheet after many times folding in different PFs gets to tear down, so to overcome this limitation, it was fabricated FPAs for different FP estimations.

The FP effect for obtaining proper V-folded FPA performance is innovatively studied. To do this, flexible substrate width increase, iteration of ground, and reconfiguring the size of PAs were considered. Apart from performance, we obtained

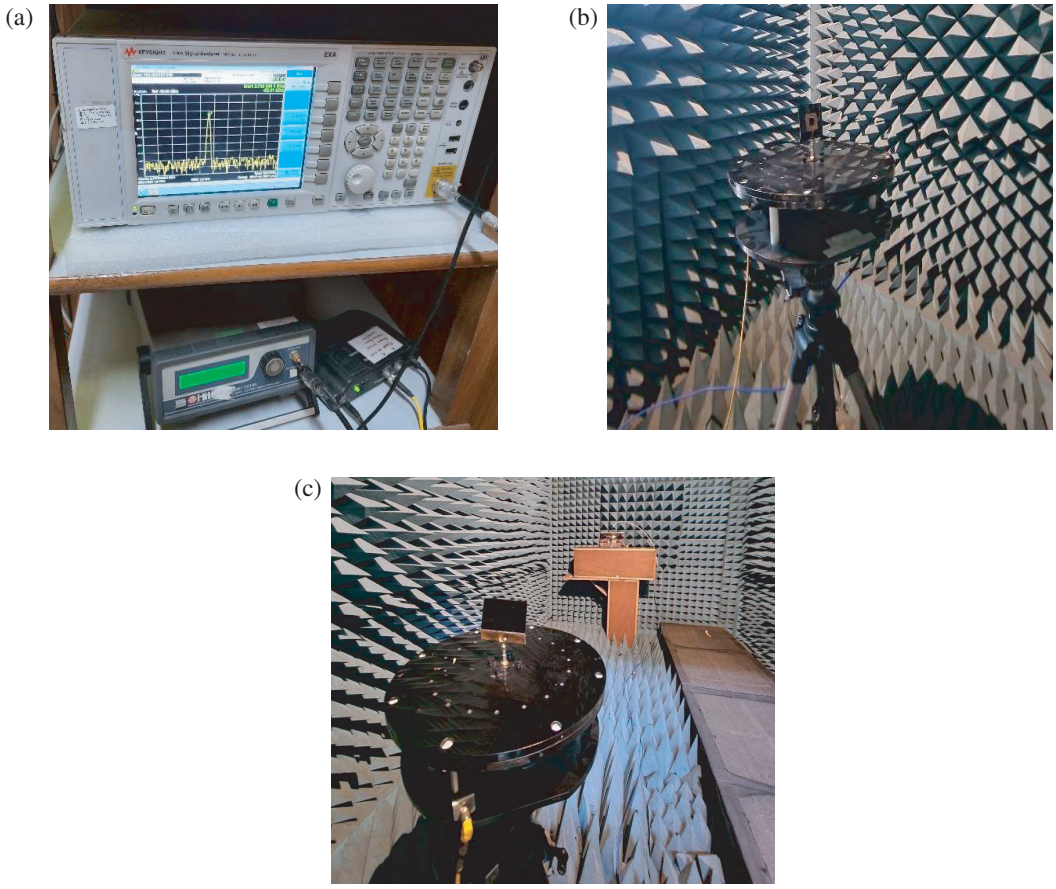

FIGURE 11. Experimental setup photos of anechoic chamber FPA tested with a signal analyzer. (b) Flat FPA, (c) Folded ($d = 10\%$) FPA.

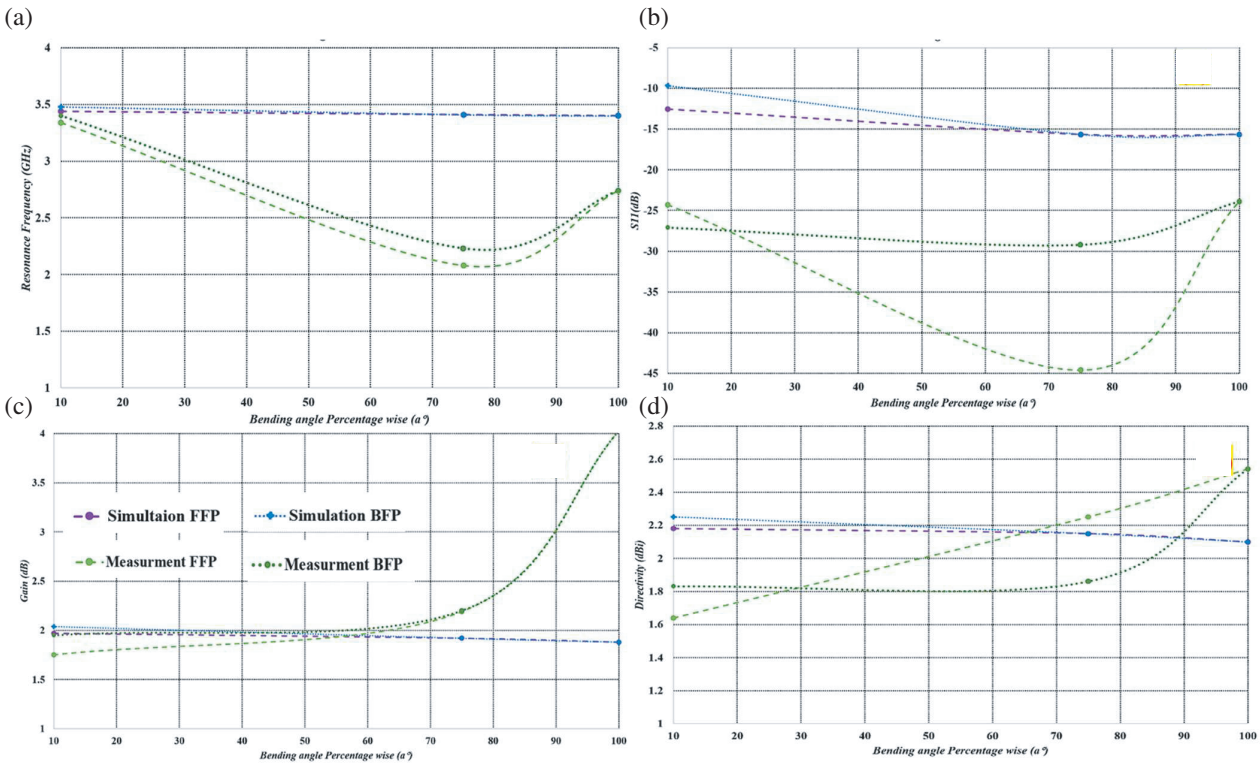

FIGURE 12. Comparison of simulation and measurement results, (a) Resonance frequency, (b) S_{11}, (c) Gain and (d) Directivity.

stabilization in the function of FP for all FFP and BFP samples. The flexible substrate thickness is 0.13 mm, but to improve performance parameters like gain, bandwidth, etc., and maintain stabilization, it was opted to increase the thickness about 4 times, i.e., 0.52 mm. The improving thickness has the advantage of holding the folding position without any support. It obtained bandwidth improvement of 10 times from the previous structure and gain improvement, so the folding antenna can be used for many applications. Designing the FPA concerning FP is challenging since no proper tools are provided for a different form of folding. Folding FPA is done by first designing the required FP structure, and molding the FPA accordingly is critical. The FFP and BFP complete samples simulated are altogether to check the folding performance.

6. CONCLUSION

In this paper, we investigate improving the performance of V-folding in PF for the complete front and back sides of FPA. The FPA needs a different form of folding in which V-folding is sharp-bent at one point, so wireless communication required for any objects can be attained. The folding of any FPA degrades performance, but after certain methods can be retained. Designing the V-fold FPA in CST MWS 2018 is challenging for about 72 samples for front and back PF simulation. This is an extensive study given for affecting performance with lumped elements changes. The simulated FPA is designed for a prototype of authenticity, and good resonance is observed. In the future, the copper sheet used for the ground plane and a radiating patch can be replaced with nanomaterial for better exhibition in folding.

ACKNOWLEDGEMENT

The present research work is supported by NSFC Grant No. 62350610268.

REFERENCES

[1] Xu, Q., B. Wang, F. Zhang, D. S. Regani, F. Wang, and K. J. R. Liu, "Wireless AI in smart car: How smart a car can be?" *IEEE Access*, Vol. 8, 55 091–55 112, 2020.

[2] Xu, G., Q. Zhang, B. Li, Y. Zhou, M. Wang, W. Feng, and Q. Zhu, "Smart car care systems and its technology prospects with service robots function," in *2014 IEEE International Conference on Information and Automation (ICIA)*, 1289–1294, Hailar, China, 2014.

[3] Miranda, J., M. Memon, J. Cabral, B. Ravelo, S. R. Wagner, C. F. Pedersen, M. Mathiesen, and C. Nielsen, "Eye on patient care: Continuous health monitoring: Design and implementation of a wireless platform for healthcare applications," *IEEE Microwave Magazine*, Vol. 18, No. 2, 83–94, 2017.

[4] Bhuva, D., K. Sathashivan, A. Patil, and S. Singh, "Smart car systems: A need in smart city," in *2018 International Conference on Smart City and Emerging Technology (ICSCET)*, 1–3, Mumbai, India, Jan. 2018.

[5] Zhao, X. and J. Jin, "High gain directional antenna array for WiMAX application," *Transactions of Tianjin University*, Vol. 20, 364–367, 2014.

[6] Song, L. and Y. Rahmat-Samii, "A systematic investigation of rectangular patch antenna bending effects for wearable applications," *IEEE Transactions on Antennas and Propagation*, Vol. 66, No. 5, 2219–2228, May 2018.

[7] Song, L. and Y. Rahmat-Samii, "Patch antenna bending effects for wearable applications: Guidelines and design curves," in *2018 United States National Committee of URSI National Radio Science Meeting (USNC-URSI NRSM)*, 1–2, Boulder, CO, USA, Jan. 2018.

[8] Sanchez-Montero, R., P.-L. Lopez-Espi, C. Alen-Cordero, and J.-A. Martinez-Rojas, "Bend and moisture effects on the performance of a U-shaped slotted wearable antenna for off-body communications in an industrial scientific medical (ISM) 2.4 GHz band," *Sensors*, Vol. 19, No. 8, 1804, 2019.

[9] Ibanez-Labiano, I., M. S. Ergoktas, C. Kocabas, A. Toomey, A. Alomainy, and E. Ozden-Yenigun, "Graphene-based soft wearable antennas," *Applied Materials Today*, Vol. 20, 100727, 2020.

[10] Kao, H.-L. and C.-H. Chuang, "Bending effects on a fabric-based antenna for wearable applications," in *2020 IEEE 70th Electronic Components and Technology Conference (ECTC)*, 1665–1670, Orlando, FL, USA, Jun. 2020.

[11] Kapetanakis, T. N., C. D. Nikolopoulos, K. Petridis, and I. O. Vardiambasis, "Wearable textile antenna with a graphene sheet or conductive fabric patch for the 2.45 GHz band," *Electronics*, Vol. 10, No. 21, 2571, 2021.

[12] Durgun, A. C., C. A. Balanis, C. R. Birtcher, and D. R. Allee, "Design, simulation, fabrication and testing of flexible bow-tie antennas," *IEEE Transactions on Antennas and Propagation*, Vol. 59, No. 12, 4425–4435, Dec. 2011.

[13] Aas, J. A. and K. Jakobsen, "Radiation patterns of rectangular microstrip antennas on finite ground planes," in *1982 12th European Microwave Conference*, 384–389, Helsinki, Finland, Sep. 1982.

[14] Li, R. L., G. DeJean, E. Tsai, E. Tentzeris, and J. Laskar, "Novel small folded shorted-patch antennas," in *IEEE Antennas and Propagation Society International Symposium (IEEE Cat. No.02CH37313)*, Vol. 4, 26–29, San Antonio, TX, USA, Jun. 2002.

[15] Olaimat, M. M. and N. I. Dib, "Improved formulae for the resonant frequencies of triangular microstrip patch antennas," *International Journal of Electronics*, Vol. 98, No. 3, 407–424, 2011.

[16] Chen, H.-D., C.-Y.-D. Sim, J.-Y. Wu, and T.-W. Chiu, "Broadband high-gain microstrip array antennas for WiMAX base station," *IEEE Transactions on Antennas and Propagation*, Vol. 60, No. 8, 3977–3980, 2012.

[17] Kumar, P. P. and R. Nakkeeran, "A new corrugated tooth like slot microstrip antenna for WiMAX/satellite applications," in *2014 IEEE Students' Conference on Electrical, Electronics and Computer Science*, 1–5, Bhopal, Mar. 2014.

[18] Pandey, R. and D. K. Vishwakarma, "A fractalized meander-line EBG-based microstrip teeth-like patch slot antenna for use in satellite and defense applications," *Microwave and Optical Technology Letters*, Vol. 58, No. 8, 2010–2015, Aug. 2016.

[19] Singh, A., M. Aneesh, Kamakshi, and J. A. Ansari, "Analysis of microstrip line fed patch antenna for wireless communications," *Open Engineering*, Vol. 7, No. 1, 279–286, 2017.

[20] Varma, R. and J. Ghosh, "Multi-band proximity coupled microstrip antenna for wireless applications," *Microwave and Optical Technology Letters*, Vol. 60, No. 2, 424–428, 2018.

[21] Ahmed, S., F. A. Tahir, A. Shamim, and H. M. Cheema, "A compact kapton-based inkjet-printed multiband antenna for flexible wireless devices," *IEEE Antennas and Wireless Propagation Let-*

ters, Vol. 14, 1802–1805, 2015.

[22] Froehle, P., T. Przybylski, C. McDonald, M. Mirzaee, S. Noghanian, and R. Fazel-Rezai, "Flexible antenna for wireless body area network," in *2015 IEEE International Symposium on Antennas and Propagation & USNC/URSI National Radio Science Meeting*, 1214–1215, Vancouver, BC, Canada, Jul. 2015.

[23] Ahmed, S., F. A. Tahir, A. Shamim, and H. M. Cheema, "A compact kapton-based inkjet-printed multiband antenna for flexible wireless devices," *IEEE Antennas and Wireless Propagation Letters*, Vol. 14, 1802–1805, 2015.

[24] Rabobason, Y. G., G. Rigas, S. Swaisaenyakorn, B. Mirkhaydarov, B. Ravelo, M. Shkunov, P. Young, and N. Benjelloun, "Design and synthesis of flexible switching 1 × 2 antenna array on Kapton substrate," *The European Physical Journal Applied Physics*, Vol. 74, No. 3, 30102, 2016.

[25] Raad, H. R., A. I. Abbosh, H. M. Al-Rizzo, and D. G. Rucker, "Flexible and compact AMC based antenna for telemedicine applications," *IEEE Transactions on Antennas and Propagation*, Vol. 61, No. 2, 524–531, Feb. 2013.

[26] Simorangkir, R. B. V. B., Y. Yang, K. P. Esselle, and B. A. Zeb, "A method to realize robust flexible electronically tunable antennas using polymer-embedded conductive fabric," *IEEE Transactions on Antennas and Propagation*, Vol. 66, No. 1, 50–58, Jan. 2018.

[27] Alharbi, S., R. M. Shubair, and A. Kiourti, "Flexible antennas for wearable applications: Recent advances and design challenges," in *12th European Conference on Antennas and Propagation (EuCAP 2018)*, 1–3, London, UK, Apr. 2018.

[28] El Gharbi, M., R. Fernández-García, S. Ahyoud, and I. Gil, "A review of flexible wearable antenna sensors: Design, fabrication methods, and applications," *Materials*, Vol. 13, No. 17, 3781, 2020.

[29] Leng, T., K. Pan, X. Zhou, Y. Li, M. A. Abdalla, and Z. Hu, "Non-volatile RF reconfigurable antenna on flexible substrate for wireless IoT applications," *IEEE Access*, Vol. 9, 119 395–119 401, 2021.

[30] Ayyala, K. A. K., A. Thakur, Z. Yong, S. S. Yazdani, P. Thakur, M. S. Prasad, N. M. Murad, S. Baccar, B. Agnus, and B. Ravelo, "Electro-geometrical analysis of transversal V-fold patch antenna," *International Journal of Electrical and Electronics Research*, Vol. 10, No. 4, 1281–1289, Dec. 2022.

[31] Ayyala, K. A. K., A. Thakur, S. Baccar, N. M. Murad, M. S. Prasad, P. Thakur, G. Fontgalland, Y. Zhou, and B. Ravelo, "Systematic flexible antenna performance study of V-folding percentage influence," *Progress In Electromagnetics Research C*, Vol. 129, 99–113, 2023.

[32] Elmobarak, H. A., M. Himdi, X. Castel, S. K. A. Rahim, and T. K. Geok, "Flexible patch antenna array operating at microwaves based on thin composite material," *IEEE Access*, Vol. 10, 115 663–115 672, 2022.

[33] Boeykens, F., L. Vallozzi, and H. Rogier, "Cylindrical bending of deformable textile rectangular patch antennas," *International Journal of Antennas and Propagation*, Vol. 2012, Article ID 170 420, 1–11, 2012.

[34] Osman, M. A. R., M. K. A. Rahim, N. A. Samsuri, M. K. Elbasheer, and M. E. Ali, "Textile UWB antenna bending and wet performances," *International Journal of Antennas and Propagation*, Vol. 2012, Article ID 251 682, 12, 2012.

[35] Phan, H. P., T.-P. Vuong, P. Benech, P. Xavier, and P. Borel, "Study of bending effects of a wideband paper-based printed microstrip-fed antenna," *Microwave and Optical Technology Letters*, Vol. 62, No. 4, 1785–1794, 2020.

[36] Mohandoss, S., S. K. Palaniswamy, R. R. Thipparaju, M. Kanagasabai, B. R. B. Naga, and S. Kumar, "On the bending and time domain analysis of compact wideband flexible monopole antennas," *AEU — International Journal of Electronics and Communications*, Vol. 101, 168–181, 2019.

[37] Boyuan, M., J. Pan, E. Wang, and Y. Luo, "Conformal bent dielectric resonator antennas with curving ground plane," *IEEE Transactions on Antennas and Propagation*, Vol. 67, No. 3, 1931–1936, Mar. 2019.

[38] Shafaet-Uz-Zaman, K. and M. A. Matin, "Analysis of bending and human body effects on sleeve-badge textile antenna performance," in *2019 TEQIP III Sponsored International Conference on Microwave Integrated Circuits, Photonics and Wireless Networks (IMICPW)*, 10–14, 2019.

[39] Balanis, C. A., *Antenna Theory: Analysis and Design*, 3rd ed., John Wiley & Sons, 2005.